Undamped low-energy plasmon in AlH_3 at high pressure

I. G. Gurtubay,[1,2,*] B. Rousseau,[2,3] and A. Bergara[1,2,3,†]

[1]*Materia Kondentsatuaren Fisika Saila, Zientzia eta Teknologia Fakultatea, Euskal Herriko Unibertsitatea, 644 Postakutxatila, Bilbo, 48080 Basque Country, Spain*

[2]*Donostia International Physics Center (DIPC), Paseo de Manuel Lardizabal, Donostia, 20018 Basque Country, Spain*

[3]*Centro de Fisica de Materiales, CSIC–UPV/EHU, 1072 Posta kutxatila, Donostia, E-20080 Basque Country, Spain*

(Received 28 June 2010; revised manuscript received 19 July 2010; published 17 August 2010)

Pressure strongly modifies electronic and optical properties of solids. In this work we report *ab initio* time-dependent density-functional theory calculations of the dielectric response of the high-pressure metallic phase of aluminum hydride (AlH_3) within the random-phase approximation. Besides the conventional free-electronlike plasmon, which is highly damped, low-energy transitions between states near the Fermi level that appear in this metallized phase give rise to a low-energy undamped collective mode. This feature is expected to induce an abrupt edge in the experimentally measured reflectivity just below 1 eV and also affect electronic correlations close to the Fermi energy. Our work shows that AlH_3 is basically a hydrogen sublattice weakly perturbed by Al atoms.

DOI: 10.1103/PhysRevB.82.085113 PACS number(s): 71.45.Gm

I. INTRODUCTION

Compressed hydrides have been the focus of many theoretical and experimental studies as candidates for high-temperature superconductors.[1] Indeed, these hydrides contain large fractions of H atoms and tend to be insulators at low pressure, while at high pressure they are expected to metallize. Since metallization of pure hydrogen has not been observed experimentally so far even at pressures as high as 340 GPa,[2–4] these hydrogen-rich materials, which are expected to metallize at considerably lower pressure, are thought to be of relevance for studying phenomena related to metallic hydrogen.

Along these lines, many hydrides such as CH_4,[5,6] SiH_4,[7–11] GeH_4,[12,13] or SnH_4 (Refs. 14 and 15) have been investigated for possible metallization at high pressures. In particular, the binary alloy aluminum hydride (AlH_3) has recently been the subject of many theoretical and experimental investigations. Pickard and Needs[16] predicted using density-functional theory (DFT) and a "random searching" technique a metallic phase of AlH_3 at 73 GPa with a structure of space group $Pm\bar{3}n$. Subsequently, Goncharenko *et al.*[17] showed experimental evidence for the pressure induced hydrogen-dense metallic state in this light covalent hydride at 100 GPa with the same symmetry predicted in Ref. 16.

Pressure is known to change the bonding and electronic properties of solids. For instance, recent calculations on compressed lithium and sodium have shown a striking departure from the classical nearly free-electronlike model behavior. In particular, calculations on the pressure-induced modification of the low-momentum dynamic electronic dielectric response function in lithium[18,19] have predicted an undamped collective mode whose absorption power gradually redistributes from the conventional plasmon to this feature. In the case of sodium, which becomes a charge-transfer insulator at high pressures, strong variations in excitonic effects are found with applied pressure. Moreover, the absorption spectrum of sodium is found to be strongly anisotropic, becoming transparent in the visible range in one polarization direction while remaining "metallic" in the other.[20,21]

Here, we focus on the study of the dynamic dielectric electronic response and optical properties of the metallic phase of AlH_3 within time-dependent DFT (TDDFT). Our *ab initio* calculations show that, for vanishing momentum transfer, the macroscopic dielectric matrix vanishes around 0.9 eV. This gives rise to a well-defined, undamped collective excitation originated in intraband electron-hole excitations but strongly affected by interband transitions. We have extended our study to an artificial system where the Al atoms in AlH_3 have been replaced with a compensating background and we have found that the resulting hydrogen sublattice has very similar electronic properties to those of AlH_3. Unless otherwise specified, atomic units are used, namely, $\hbar = m_e = e^2 = 4\pi\epsilon_0 = 1$.

II. THEORY

The starting point of our calculations is a set of well-converged Bloch states $\phi_{n\mathbf{k}}$ and energies $\varepsilon_{n\mathbf{k}}$, which are the eigenfunctions and eigenvalues of the Kohn-Sham equation of DFT. Then we evaluate the density-response function $\chi^0(\mathbf{r},\mathbf{r}',\omega)$ of noninteracting electrons moving in the effective Kohn-Sham potential.[22] Given the lattice periodicity of the solid, the Fourier transform of χ^0 with respect to space coordinates can be expressed as

$$\chi^0_{\mathbf{G},\mathbf{G}'}(\mathbf{q},\omega) = \frac{1}{\Omega}\sum_{\mathbf{k}}^{1\mathrm{BZ}}\sum_{n,n'}\frac{f(\xi_{n\mathbf{k}}) - f(\xi_{n'\mathbf{k}+\mathbf{q}})}{\xi_{n\mathbf{k}} - \xi_{n'\mathbf{k}+\mathbf{q}} + \omega + i\eta} \times \langle n\mathbf{k}|e^{-i(\mathbf{q}+\mathbf{G})\cdot\mathbf{r}}|n'\mathbf{k}+\mathbf{q}\rangle\langle n'\mathbf{k}+\mathbf{q}|e^{i(\mathbf{q}+\mathbf{G}')\cdot\mathbf{r}}|n\mathbf{k}\rangle, \quad (1)$$

where Ω represents the normalization volume, $\mathbf{k}$ and $\mathbf{q}$ are wave vectors within the first Brillouin zone (1BZ), $\mathbf{G}$ and $\mathbf{G}'$ are reciprocal lattice vectors, η is a positive infinitesimal, $\xi_{n\mathbf{k}} = \varepsilon_{n\mathbf{k}} - \varepsilon_F$, and $f(\xi)$ is the Fermi occupation function.

In the framework of TDDFT,[23] the Fourier coefficients of the density-response function of interacting electrons, $\chi(\mathbf{r},\mathbf{r}',\omega)$, are given by

$$\chi_{\mathbf{G},\mathbf{G}'}(\mathbf{q},\omega) = \chi^0_{\mathbf{G},\mathbf{G}'}(\mathbf{q},\omega) + \sum_{\mathbf{G}_1,\mathbf{G}_2} \chi^0_{\mathbf{G},\mathbf{G}_1}(\mathbf{q},\omega)\{v_{\mathbf{G}_1}(\mathbf{q})\delta_{\mathbf{G}_1,\mathbf{G}_2} + f^{\mathrm{XC}}_{\mathbf{G}_1,\mathbf{G}_2}[n_0](\mathbf{q},\omega)\}\chi_{\mathbf{G}_2,\mathbf{G}'}(\mathbf{q},\omega), \quad (2)$$

where $v_{\mathbf{G}}(\mathbf{q})=4\pi/|\mathbf{q}+\mathbf{G}|^2$ is the Fourier transform of the bare Coulomb potential and $f^{\mathrm{XC}}_{\mathbf{G},\mathbf{G}'}[n](\mathbf{q},\omega)$ are the Fourier coefficients of the functional derivative of the time-dependent exchange-correlation (XC) potential of TDDFT, which accounts for the dynamical XC effects.

The inverse dielectric matrix, whose negative imaginary part, $-\mathrm{Im}[\epsilon^{-1}_{\mathbf{G},\mathbf{G}'}(\mathbf{q},\omega)]$, yields the loss function, is given in terms of χ by

$$\epsilon^{-1}_{\mathbf{G},\mathbf{G}'}(\mathbf{q},\omega) = \delta_{\mathbf{G},\mathbf{G}'} + v_{\mathbf{G}}(\mathbf{q})\chi_{\mathbf{G},\mathbf{G}'}(\mathbf{q},\omega). \quad (3)$$

The macroscopic dielectric function is defined as

$$\epsilon_M(\mathbf{q},\omega) = 1/\epsilon^{-1}_{\mathbf{0},\mathbf{0}}(\mathbf{q},\omega), \quad (4)$$

where $\epsilon^{-1}_{\mathbf{0},\mathbf{0}}(\mathbf{q},\omega)$ represents the first diagonal element of the inverse dielectric matrix of Eq. (3). In the absence of crystal local-field effects, which arise when the microscopic electric field varies rapidly over the unit cell,[24] the off-diagonal elements of the inverse dielectric matrix are negligible and the macroscopic dielectric function coincides, therefore, with the first diagonal element of the dielectric matrix. In the random-phase approximation (RPA), which neglects XC effects [$f^{\mathrm{XC}}=0$ in Eq. (2)], the dielectric matrix is given by

$$\epsilon^{\mathrm{RPA}}_{\mathbf{G},\mathbf{G}'}(\mathbf{q},\omega) = \delta_{\mathbf{G},\mathbf{G}'} - v_{\mathbf{G}}(\mathbf{q})\chi^0_{\mathbf{G},\mathbf{G}'}(\mathbf{q},\omega). \quad (5)$$

Collective excitations (plasmons) occur at energies where both the real and the imaginary parts of the macroscopic dielectric function are zero. The normal-incidence reflectivity R is defined as

$$R = \frac{(n-1)^2+\kappa^2}{(n+1)^2+\kappa^2}, \quad (6)$$

where the index of refraction, n, and the extinction coefficient, κ, are related to the real and imaginary parts of the macroscopic dielectric function for $\mathbf{q}\to\mathbf{0}$ through the equations

$$\mathrm{Re}\ \epsilon_M = n^2 - \kappa^2 \quad (7)$$

and

$$\mathrm{Im}\ \epsilon_M = 2n\kappa. \quad (8)$$

III. RESULTS AND DISCUSSION

Our *ab initio* calculations are based on the $Pm\bar{3}n$ structure characterized in Ref. 17 at 110 GPa. We adopt an all-electron approach where $\phi_{n\mathbf{k}}$ and $\varepsilon_{n\mathbf{k}}$ were obtained using the generalized gradient approximation (GGA) (Ref. 25) of the exchange-correlation potential by means of the full potential linearized augmented plane wave method[26] using a RKMAX=7 cutoff criterion. The muffin-tin radius of Al and H was set to 2.1 and 1.3, respectively. The dielectric function was obtained by using a $30\times30\times30$ mesh in reciprocal space, including states up to 68 eV above the Fermi energy and a damping of 0.03 eV in Eq. (1).[27] We restrict our attention to the RPA response[28] of AlH_3 at the low-energy range and vanishing momentum transfer ($\mathbf{q}\to\mathbf{0}$), where LFE[29] and dynamical XC effects are negligible.

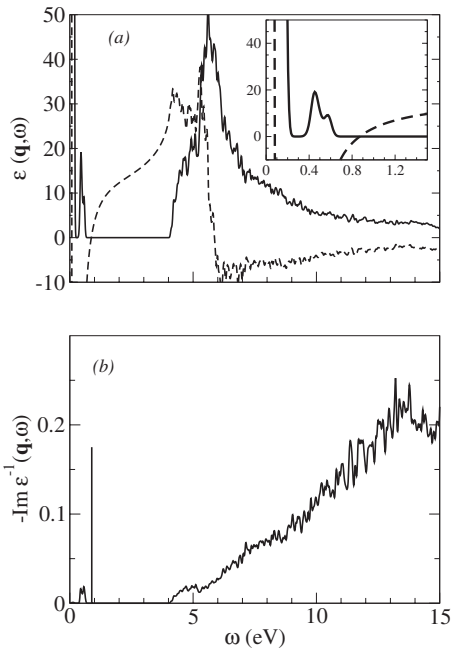

FIG. 1. Dielectric properties of AlH_3 for $|\mathbf{q}|\to0$ [$\mathbf{q}=1/100\times(100)$]. (a) The real (dashed line) and imaginary (solid line) parts of the macroscopic RPA dielectric function. (b) The corresponding loss function. The vertical line represents the δ peak corresponding to the undamped low-energy plasmon.

The solid and dashed lines in Fig. 1(a) show the imaginary and real parts of the dielectric function for $\mathbf{q}=1/100\times(100)$ within the RPA. The diagonal elements of the imaginary part of the RPA dielectric matrix are known to represent a measure of the number of states available for real transitions involving a given momentum transfer $\mathbf{q}$ and energy transfer ω. Below 1 eV, Im ϵ shows two sharp peaks, one centered at about 0.1 eV and another one with a double-hump structure between 0.4 and 0.65 eV [see inset of Fig. 1(a)] which reflect the availability for single-particle transitions close to the Fermi level.

The Kramers-Kronig relations between the real and imaginary parts of the macroscopic dielectric function guarantee that the real part has a "dip" whenever the imaginary part has a "jump." Because both the real part (dashed line) and the imaginary part (solid line) vanish around 0.9 eV, a well-defined, undamped plasmon peak builds up around this energy. This plasmon cannot decay via single-particle excitations so it has a very long lifetime as shown by the δ function in the energy-loss function displayed in Fig. 1(b).

The features observed in the response function have their origin in the band structure, which is shown in Fig. 2 along with the density of states of AlH_3. At an intuitive level, two main features are to be expected. First, there should be a conventional free-electronlike plasmon; the simplest approximation for its frequency in the case of AlH_3 is $\omega_p=\sqrt{4\pi\rho}\simeq23.8$ eV, thus placing it squarely in the range of

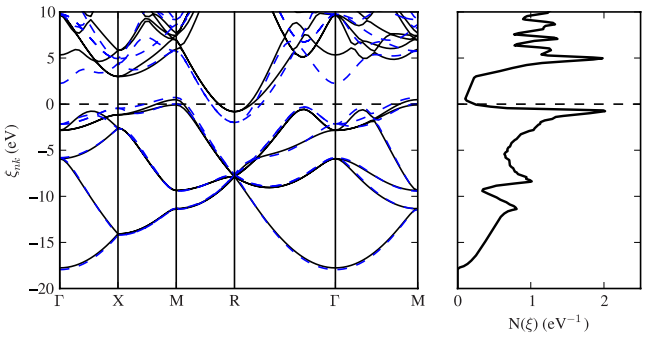

FIG. 2. (Color online) Left panel: bands of AlH_3 (full black line) and of the hypothetical system composed of the hydrogen subsystem immersed in a jellium background (dashed blue line), near the Fermi energy. Right panel: density of states of AlH_3 per unit cell.

electron-hole excitations, leading to large damping by single-particle transitions. Second, the fact that the system is a metal with small hole pockets around M and an electron pocket around R produces a second, low-energy plasmon. To get a sense of scale, a simple two fluids (electrons and holes) analysis and an effective mass description of the relevant bands suggest that this intraband plasmon should have frequency $\simeq$3.5 eV, outside the energy range where electron-hole excitations provide decay channels. These energies are higher than the energies of the peaks associated to the plasmons in the loss function of Fig. 1(b) (14.5 eV and 0.9 eV, respectively), the shift corresponding to the screening associated to the interband electron-hole excitation not included in the simple free-electron picture.

A careful analysis of all possible initial and final states contributing to χ^0 in Eq. (1) shows that the origin of the first peak are intraband transitions between electronic states close to the R and the M points while the second peak stems exclusively from interband transitions between states around the M point. Furthermore, the band structure shows a gap for nearly vertical transitions of about 4 eV for all initial states with energies lower than −0.7 eV, which translates into a flat (zero) region in Im ϵ. For energy transfers larger than this gap, the continuum of single-particle transitions gives rise to the broad peak starting at 4 eV, corresponding to the onset of excitations around X.

In order to better understand the role of the H atoms in AlH_3, the band structure of an hypothetical system composed of only the hydrogen sublattice and a compensating background charge was computed (henceforth this will be referred to as the "hydrogen subsystem"). As can be seen in Fig. 2, the bands of AlH_3 and of the hydrogen subsystem are qualitatively very similar below the Fermi energy. Near the Fermi energy, the presence of aluminum shifts the bands up at the R point and down at the X point while leaving them almost unchanged at M. Furthermore, two nearly parallel bands arise in the XM and ΓM directions in the hydrogen subsystem. It is straightforward to understand the effect of the presence or absence of aluminum on the band structure by considering the contribution to the total electronic density coming from states of interest.[30] The density contribution from the states immediately below the Fermi energy at the R

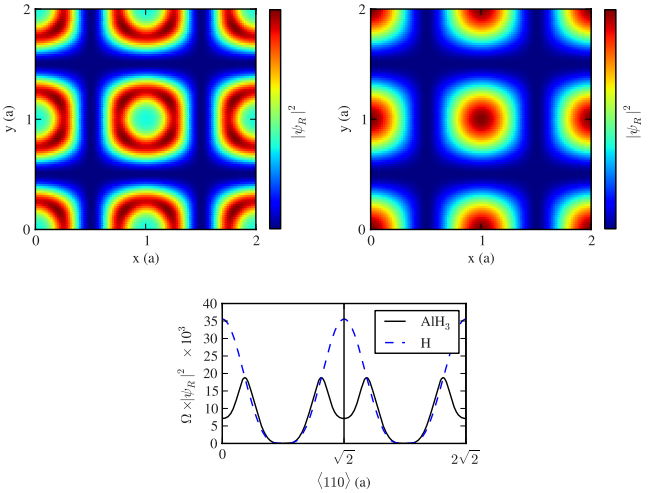

FIG. 3. (Color online) Electronic density contribution from the R point. The density on the {100} plane for AlH_3 (upper left) and for the hydrogen system (upper right). Comparison of the densities for the two systems in the ⟨110⟩ direction (bottom). The vertical lines indicate the positions of the aluminum sites. Many periodic repetitions are shown for clarity.

point can be seen in Fig. 3. In the absence of aluminum, electronic charge piles up at what would be the aluminum sites. When these ions are present, the density profile is modified because of aluminum's repulsive ionic core and the energy associated with these states is higher. Similarly, the density contributions from states near the Fermi energy at the M point (not shown) vanish at the aluminum sites (whether the metallic ions are present or not), thus making these eigenstates and their corresponding eigenvalues qualitatively oblivious to the presence of the metallic ions.

Figure 4 shows the real and imaginary parts of the dielectric function of the hydrogen sublattice system together with those of AlH_3. As expected, the peak stemming from interband transitions around the Fermi level is slightly shifted to higher energies and broadened according to the change in the bands in the hydrogen sublattice when approaching M from X and Γ. Otherwise, both systems show qualitatively very similar dielectric functions at low energies, in agreement with our previous conclusions, i.e., that AlH_3 is mainly a hydrogen sublattice very weakly disturbed by the presence of Al atoms.

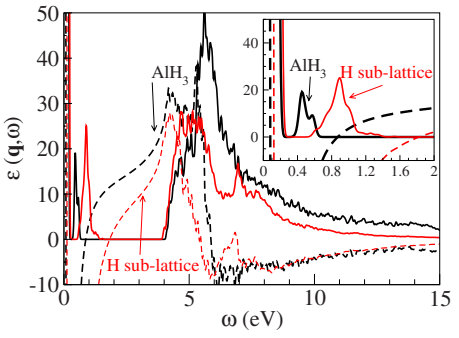

FIG. 4. (Color online) Real (solid) and imaginary (dashed) parts of the dielectric function of AlH_3 (black) and the hydrogen sublattice with a compensating background (red) for $|\mathbf{q}|$=0.011 a.u.$^{-1}$

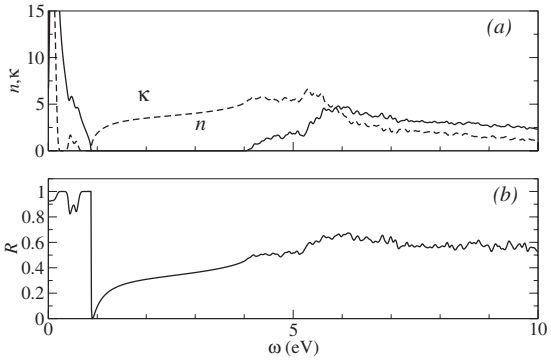

FIG. 5. Optical properties of AlH_3 for $|\mathbf{q}|=0.011$ a.u.$^{-1}$ computed from the dielectric function of Fig. 1(a). (a) Extinction coefficient (dashed line) and refraction index (solid line). (b) Reflectivity. The reflectivity vanishes at the undamped plasmon energy.

The effect of the collective excitation predicted around 1 eV is susceptible to observation through optical measurements.[31] Figure 5 shows the refraction index, n, extinction coefficient, κ, and reflectance, R, of AlH_3 derived from the macroscopic dielectric function. Our calculations show that incident light with frequency slightly above the plasmon frequency should experience an abrupt decrease in reflectivity with the subsequent near total loss of reflectivity at about 0.9 eV. The dip in R at the plasmon frequency is followed by a broader region which reaches a local maximum of 0.6 around 6 eV.

IV. SUMMARY AND CONCLUSIONS

We have calculated the dielectric and optical properties of the metallic phase of AlH_3 at 110 GPa. We have found that for vanishing momentum transfer the real and imaginary parts of the dielectric functions vanish simultaneously giving rise to an undamped plasmon at 0.9 eV. We have demonstrated that its energy is strongly affected by the onset of the continuum of interband transitions at 4 eV. This plasmon just below 1 eV should induce an abrupt decrease in the reflectivity which should be measurable.

ACKNOWLEDGMENTS

This work was partially supported by the University of the Basque Country UPV/EHU and the Basque Government (Grants No. GIC07IT36607 and No. IT-366-07), as well as the Spanish Ministerio de Educación y Ciencia (Grant No. FIS2009-09631). Computing facilities were provided by the SGI/IZO-SGIker UPV/EHU (supported by the National Program for the Promotion of Human Resources within the National Plan of Scientific Research, Development and Innovation-Fondo Social Europeo, MCyT and the Basque Government) and by the Donostia International Physics Center (DIPC) foundation. I.G.G is grateful to C. Ambrosch-Draxl and her group for technical assistance with the WIEN2K package "Excitonic effects in semiconductors."

*idoia.gurtubay@ehu.es
†a.bergara@ehu.es

[1] N. W. Ashcroft, Phys. Rev. Lett. **92**, 187002 (2004).
[2] H. Mao and R. J. Hemley, Rev. Mod. Phys. **66**, 671 (1994).
[3] P. Loubeyre, F. Occelli, and R. LeToullec, Nature (London) **416**, 613 (2002).
[4] K. Nagao, S. A. Bonev, A. Bergara, and N. W. Ashcroft, Phys. Rev. Lett. **90**, 035501 (2003).
[5] M. Martinez-Canales and A. Bergara, High Press. Res. **26**, 369 (2006).
[6] L. Sun, W. Yi, L. Wang, J. Shu, S. Sinogeikin, Y. Meng, G. Shen, L. Bai, Y. Li, J. Liu, H.-k. Mao, and W. L. Mao, Chem. Phys. Lett. **473**, 72 (2009).
[7] J. Feng, W. Grochala, T. Jaron, R. Hoffmann, A. Bergara, and N. W. Ashcroft, Phys. Rev. Lett. **96**, 017006 (2006).
[8] C. J. Pickard and R. J. Needs, Phys. Rev. Lett. **97**, 045504 (2006).
[9] Y. Yao, J. S. Tse, Y. Ma, and K. Tanaka, EPL **78**, 37003 (2007).
[10] O. Degtyareva, M. Martínez Canales, A. Bergara, X.-J. Chen, Y. Song, V. V. Struzhkin, H.-k. Mao, and R. J. Hemley, Phys. Rev. B **76**, 064123 (2007).
[11] M. Martinez-Canales, A. R. Oganov, Y. Ma, Y. Yan, A. O. Lyakhov, and A. Bergara, Phys. Rev. Lett. **102**, 087005 (2009).
[12] M. Martinez-Canales, A. Bergara, J. Feng, and W. Grochala, J. Phys. Chem. Solids **67**, 2095 (2006).
[13] G. Gao, A. R. Oganov, A. Bergara, M. Martinez-Canales, T. Cui, T. Iitaka, Y. Ma, and G. Zou, Phys. Rev. Lett. **101**, 107002 (2008).
[14] J. S. Tse, Y. Yao, and K. Tanaka, Phys. Rev. Lett. **98**, 117004 (2007).
[15] G. Gao, A. R. Oganov, P. Li, Z. Li, H. Wang, T. Cui, Y. Ma, A. Bergara, A. O. Lyakhov, T. Iitaka, and G. Zou, Proc. Natl. Acad. Sci. U.S.A. **107**, 1317 (2010).
[16] C. J. Pickard and R. J. Needs, Phys. Rev. B **76**, 144114 (2007).
[17] I. Goncharenko, M. I. Eremets, M. Hanfland, J. S. Tse, M. Amboage, Y. Yao, and I. A. Trojan, Phys. Rev. Lett. **100**, 045504 (2008).
[18] V. M. Silkin, A. Rodriguez-Prieto, A. Bergara, E. V. Chulkov, and P. M. Echenique, Phys. Rev. B **75**, 172102 (2007).
[19] A. Rodriguez-Prieto, V. M. Silkin, A. Bergara, and P. M. Echenique, New J. Phys. **10**, 053035 (2008).
[20] A. Lazicki, A. F. Goncharov, V. V. Struzhkin, R. E. Cohen, Z. Liu, E. Gregoryanz, C. Guillaume, H.-K. Mao, and R. J. Hemley, Proc. Natl. Acad. Sci. U.S.A. **106**, 6525 (2009).
[21] M. Gatti, I. V. Tokatly, and A. Rubio, Phys. Rev. Lett. **104**, 216404 (2010).
[22] The density-response function of a many-electron system yields the electron density induced at a given point of space by an arbitrary (small) frequency-dependent external potential.
[23] M. Petersilka, U. J. Gossmann, and E. K. U. Gross, Phys. Rev. Lett. **76**, 1212 (1996).
[24] S. L. Adler, Phys. Rev. **126**, 413 (1962).
[25] J. P. Perdew, K. Burke, and M. Ernzerhof, Phys. Rev. Lett. **77**, 3865 (1996).

[26] P. Blaha, K. Schwarz, G. K. Madsen, and J. Luitz, *Computer Code WIEN2k* (Technical University of Vienna, Vienna, 2009).

[27] Calculations with RKMAX=9, different muffin-tin radii for Al and H and samplings of the BZ of $16\times16\times16$ and $20\times20\times20$ show that our calculations are converged within the energy range considered.

[28] The response was obtained using the program package from WIEN2K "Excitonic effects in semiconductors" contributed by Peter Puschnig.

[29] Crystal LFE arise because the microscopic electric field varies rapidly over the unit cell. As a result, the polarization due to an external perturbation will in general contain rapidly varying terms with wave vector $\mathbf{q}+\mathbf{G}$, which are described by the off-diagonal elements of the dielectric matrix (see Ref. 24).

[30] In order to compute the pseudoelectronic densities associated with various states, electronic properties were computed using DFT as implemented in the QUANTUM-ESPRESSO package (Ref. 32). The exchange correlation was treated using the GGA of Perdew, Burke, and Ernzerhof (Refs. 25 and 33). Ultrasoft pseudopotentials (Ref. 34) were used, where $3s$ and $3p$ states of aluminium were treated as valence. The plane-wave basis cutoff was set to 80 Ry. First Brillouin-zone integrations were performed as sums on a $16\times16\times16$ Monkhorst-Pack (Ref. 35) $\mathbf{k}$ mesh, using a smearing parameter of 20 mRy. The band structure obtained in this fashion was indistinguishable from the band structure obtained using WIEN2K in the vicinity of the Fermi energy, thus providing a good consistency check of both methods.

[31] Raman and visible absorption spectra of AlH_3 have been reported only very recently for pressures up to 50 GPa. See Ref. 36.

[32] P. Giannozzi, S. Baroni, N. Bonini, M. Calandra, R. Car, C. Cavazzoni, D. Ceresoli, G. L. Chiarotti, M. Cococcioni, I. Dabo, A. Dal Corso, S. de Gironcoli, S. Fabris, G. Fratesi, R. Gebauer, U. Gerstmann, C. Gougoussis, A. Kokalj, M. Lazzeri, L. Martin-Samos, N. Marzari, F. Mauri, R. Mazzarello, S. Paolini, A. Pasquarello, L. Paulatto, C. Sbraccia, S. Scandolo, G. Sclauzero, A. P. Seitsonen, A. Smogunov, P. Umari, and R. M. Wentzcovitch, J. Phys.: Condens. Matter **21**, 395502 (2009).

[33] J. P. Perdew, K. Burke, and M. Ernzerhof, Phys. Rev. Lett. **78**, 1396 (1997).

[34] D. Vanderbilt, Phys. Rev. B **41**, 7892 (1990).

[35] H. J. Monkhorst and J. D. Pack, Phys. Rev. B **13**, 5188 (1976).

[36] N. Shimura, T. Takeichi, T. Kume, S. Sasaki, H. Shimizu, A. Ohmura, K. Ikeda, and Y. N. S. Orimo, J. Phys.: Conf. Ser. **215**, 012047 (2010).